Chemical Science

ROYAL SOCIETY OF CHEMISTRY

EDGE ARTICLE

View Article Online
View Journal | View Issue

Cite this: *Chem. Sci.*, 2020, **11**, 5565

All publication charges for this article have been paid for by the Royal Society of Chemistry

Received 9th February 2020
Accepted 11th May 2020

DOI: 10.1039/d0sc00770f

rsc.li/chemical-science

A polycyclic aromatic hydrocarbon diradical with pH-responsive magnetic properties†

Xiangyu Fu,‡ Han Han,‡ Di Zhang, Han Yu, Qilin He and Dahui Zhao *

By integrating azulene with a quinoid moiety, a novel non-alternant polycyclic aromatic hydrocarbon molecule **BCHF1** exhibiting manifold zwitterionic, quinoidal and diradical behaviors is designed and synthesized. Its zwitterionic feature is evidenced by the changes shown by the ^{1}H-NMR and absorption spectra when the molecule undergoes reversible protonation and deprotonation reactions at varied pH. The diradical facet, manifesting a small singlet–triplet energy gap (ΔE_{S-T}), is characterized with a paramagnetic resonance signal detected by the EPR spectroscopy at room temperature. As the diradical properties are not observed in the protonated form, **BCHF1+H$^+$**, a pH-controlled reversible magnetic switching behavior is illustrated by monitoring the on and off cycles of EPR signals upon successively adding bases and acids to a solution or exposing a thin film of **BCHF1+H$^+$** to base vapor followed by acid vapor.

Introduction

Owing to the unique properties conferred by the magnetic spin and open-shell electronic feature, organic radicals have attracted growing research interest as emerging functional materials with potential applications in diverse fields, including molecular magnetism,[1,2] magneto- and opto-electronics,[3–7] *etc.* Among the various capacities, molecules exhibiting different spin states and thus switchable magnetic properties responsive to external stimuli, such as light,[8–10] temperature,[3,11–14] pH[15,16] and redox conditions,[17] are of special value.[18–23] The major challenge in developing functional materials lies in the evasive nature and low stability of organic (poly)radicals, due to their open-shell electronic characteristics. Compared to the light hetero-atom (N or O) analogues, polycyclic aromatic hydrocarbon (PAH) polyradicals are even more difficult to stabilize. Nonetheless, owing to their unique optical, electronic and magnetic properties which are valuable to versatile applications,[24,25] continual research endeavours are made for designing and synthesizing new persistent PAH radicals, and tremendous progress has been witnessed in past decades.[26–30] In particular, devising suitably extended polycyclic quinoidal scaffolds has been demonstrated as an effective strategy to induce the open-shell diradical state, by gaining stabilizing energy from aromatizing multiple quinoid rings.

Among the different stimulating mechanisms, we are interested in developing a pH-sensitive molecular magnetic switch by harnessing the diradical–quinoidal bistable states. This necessarily entails integrating a pH-responsive unit with a hydrocarbon moiety capable of swapping between the open-shell and closed-shell electronic structures. To this end, azulene[31–36] attracted our attention for possessing a unique bicyclic zwitterionic scaffold (Fig. 1a) comprising an electron-rich five-membered ring which is capable of reversible protonation

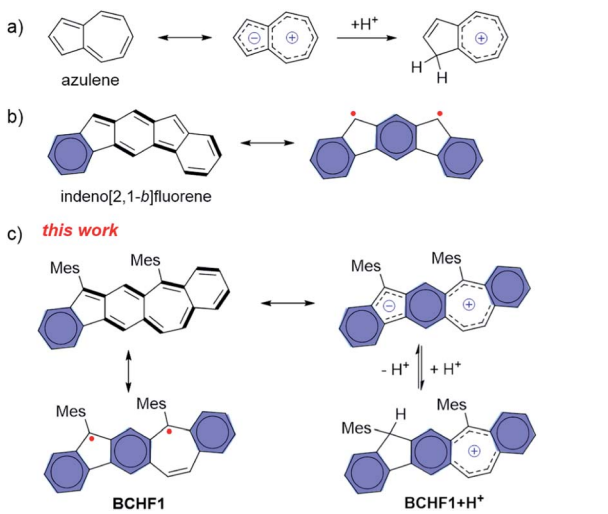

Fig. 1 (a) Azulene and its protonated form; (b) indeno[2,1-*b*]fluorene with a distinct diradical feature; (c) quinoidal, zwitterionic, diradical and protonated forms of **BCHF1**.

Beijing National Laboratory for Molecular Sciences, Centre for the Soft Matter Science and Engineering, Key Lab of Polymer Chemistry & Physics of the Ministry of Education, College of Chemistry, Peking University, Beijing, 100871, China. E-mail: dhzhao@pku.edu.cn

† Electronic supplementary information (ESI) available: Synthesis details, additional spectroscopic data, and DFT calculations. CCDC 1982861. For ESI and crystallographic data in CIF or other electronic format see DOI: 10.1039/d0sc00770f

‡ These authors contributed equally to this work.

under suitable pH conditions.[37–39] We thus propose that, by integrating the azulene skeleton with a quinoid moiety, a diradical molecule equipped with a zwitterionic feature may be devised, and hence a pH-responsive magnetic capacity is attained. Based on these considerations, we design **BCHF1**, which consists of a polycyclic benzo[5,6]cyclohepta[1,2-*b*]fluorene framework. That is, a quinoid moiety is fused in-between the 5- and 7-membered rings of azulene and thereby a novel PAH manifesting three different resonance forms of diradical, quinoidal and zwitterionic features is created. Among the three states, the quinoidal form exhibits only one Clar sextet. Yet, the diradical possesses three of such sextets, and the zwitterion gains further stabilizing energy from the pseudo-aromatization of the five- and seven-membered-ring moieties, besides three benzene sextets. Hence, the molecule is expected to manifest more pronounced diradical and zwitterionic properties, bestowing the designed pH-responsive magnetic-switching capability (Fig. 1c).

Interestingly, in comparison to **BCHF1**, its regio-isomeric molecule benzo[4,5]cyclohepta[1,2-*b*]fluorene (**BCHF2**, Scheme 1), which was previously synthesized and studied by Chi and Miao *et al.*,[40] was shown to be a stable compound with no evident diradical properties. Distinct diradical properties are anticipated in **BCHF1** and **BCHF2**, by drawing analogy with a pair of indenofluorene (IF) isomers,[27,41–45] indeno[1,2-*b*]fluorene and indeno[2,1-*b*]fluorene. According to previous studies,[43] indeno[2,1-*b*]fluorene exhibits pronounced open-shell characteristics (Fig. 1b), by displaying a large diradical component (y) of 0.65 with a small singlet–triplet energy gap (ΔE_{S-T}), whereas indeno[1,2-*b*]fluorene is shown to be a closed-shell molecule (y = 0.26) with a dominant quinoid structure.[44] Such disparate behaviours are attributed to the extra Clar sextet gained by indeno[2,1-*b*]fluorene compared to indeno[1,2-*b*]fluorene, upon transforming from a quinoidal to a diradical form. This additional aromatizing energy helps stabilize the diradical state of indeno[2,1-*b*]fluorene. On the basis of these findings with IF isomers, we speculate that such contrasting diradical behaviours should similarly be manifested by the benzocycloheptafluorene isomers. That is, as an analogue of indeno[2,1-*b*]fluorene, **BCHF1** would possess more pronounced diradical character with a smaller ΔE_{S-T} than **BCHF2**, which is an analogue of indeno[1,2-*b*]fluorene.

Moreover, one extra Clar sextet is also acquired by the zwitterionic form of **BCHF1** compared to **BCHF2**, relative to their respective quinoidal states. Therefore, a more pronounced charge separation feature is also expectable from **BCHF1** than **BCHF2**, which should enable more facile protonation of the zwitterionic form of **BCHF1**, resembling the properties of azulene. As the paramagnetic state of **BCHF1** is switched "off" upon protonation, for eliminating the diradical resonance (Fig. 1c), superior pH sensitivity and magnetic-switching capability can thus be achieved.

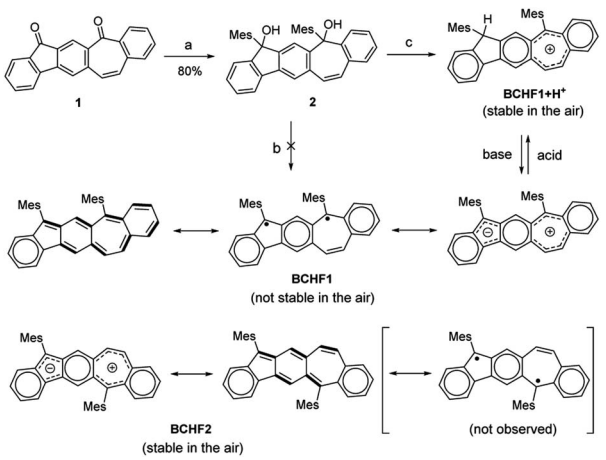

Scheme 1 Chemical structures and synthetic routes. Reactions and conditions: (a) MesLi, THF; (b) $SnCl_2$, ethyl acetate; (c) $BF_3 \cdot Et_2O$, Et_3SiH, CH_2Cl_2.

Results and discussion

DFT calculations

Computational simulations were conducted to analyze and compare the properties of **BCHF1** and **BCHF2**. The calculations were conducted at the level of (U)B3LYP/6-311G(d). The calculation results very well supported our hypothesis that **BCHF1** should possess significant open-shell characters, and a small singlet–triplet energy gap ($\Delta E_{S-T} = E_S - E_T$, where E_S and E_T represent the energy of the open-shell singlet and triplet, respectively) of merely -1.84 kcal mol^{-1} (Table S1†) was predicted, which was sufficiently small for the existence triplet species around room temperature. In comparison, a closed-shell structure with a much larger ΔE_{S-T} of -18.49 kcal mol^{-1} was obtained with **BCHF2**. Moreover, evident differences were also noted with the highest occupied molecular orbital (HOMO) and lowest unoccupied molecular orbital (LUMO). While both HOMO and LUMO of **BCHF2** were much delocalized over the entire polycyclic framework, the HOMO of **BCHF1** was fairly localized to the fluorene moiety and the LUMO was mainly distributed among the seven-membered ring and two fused benzene units (Fig. S10†). Such more localized charge distribution predicted for **BCHF1** was verified by a considerably larger dipole moment (4.75 D) calculated for **BCHF1** than **BCHF2** (2.76 D). Such properties evidently demonstrated the more pronounced charge separation feature of **BCHF1**. Therefore, all these calculation results basically proved that, because of the extra Clar sextet gained by the zwitterionic and diradical states of **BCHF1** than **BCHF2**, compared to their respective quinoidal forms, the diradical and zwitterionic forms are more important than the quinoidal form in **BCHF1**, whereas the quinoidal form is comparatively more significant in **BCHF2**, which was confirmed by its crystallographic data.[40]

Synthesis and structural characterization

Based on the above molecular design and calculation results, we set out to synthesize and investigate the properties of **BCHF1**, with **BCHF2** examined for comparison. The preparation of **BCHF1** was first attempted by adapting a similar synthetic route previously developed for **BCHF2**.[40] Specifically, dione **1** (Scheme

1) was obtained from 6-phenethyl-4-phenyl substituted *m*-phthalate *via* dual intramolecular Friedel–Crafts acylation, followed by bromination and elimination to convert the ethylene linker to a conjugated vinylene bridge (see the ESI†). Then, by carrying out a double nucleophilic addition to dione **1** with mesityllithium, diol **2** was obtained as a direct precursor to **BCHF1**. However, when a commonly applied reductive reagent tin(II) chloride was used to reduce diol **2**, we were not able to isolate **BCHF1**. In order to confirm that the synthetic procedures were suitably performed, we independently prepared the regio-isomer **BCHF2** and found that under the same conditions **BCHF2** was successfully obtained as a green solid from analogous substrates. The structure of **BCHF2** was verified by comparing the characterization data to those reported in the literature.[40] Then, the molecule was confirmed to be diamagnetic by its silent electron-paramagnetic resonance (EPR) spectrum and the quite normal NMR signals. The molecule was also observed to display adequate stability under ambient conditions.

As the reducing protocol using $SnCl_2$ did not provide the desired molecule **BCHF1**, alternative reducing conditions were employed. After diol **2** was subjected to reaction with Et_3SiH in the presence of Lewis acid $BF_3 \cdot Et_2O$ and maintained at 0 °C for about an hour, a substantial amount of red precipitation was observed upon solvent evaporation. Besides the disparate colour, the ^{1}H NMR spectrum of this red product was evidently dissimilar to that of **BCHF2**. While all 16 aromatic and vinylic protons were detected in a relatively narrow chemical shift range of 6.4 to 7.6 ppm with **BCHF2** (see the ESI†), a set of resonance signals shown by this red compound were found to range widely from 5.6 to 9.6 ppm (Fig. 2a). Although the appearance of both up- and down-field shifted signals was initially suspected to arise from the zwitterionic feature of **BCHF1**, inconsistency emerged unambiguously when 17 rather than 16 proton resonances were identified between 5 and 10 ppm. While this observation ruled out the possibility that the red product was the simple form of **BCHF1**, subsequently performed high-resolution mass spectrometry confirms the presence of an ion peak corresponding to the molecular mass of **BCHF1+H$^+$**. Combined with the ^{1}H NMR data, we concluded that the red compound was a protonated salt of **BCHF1** (*i.e.*, **BCHF1+H$^+$**).

The formation of such a protonated structure was plausible considering the reduction mechanism of triethylsilane, which offered a hydride upon the Lewis acid-facilitated removal of both hydroxide groups from diol **2**. The reduction by a second hydride did not occur likely because of the high stability of the cationic aromatic species **BCHF1+H$^+$**, which boasted a seven-membered ring hosting 6 electrons. Moreover, reasonable assignments were made for all 17 proton signals detected in the aromatic regime of the ^{1}H NMR spectrum (Fig. 2a). The furthest up-field shifted singlet at about 5.6 ppm was ascribed to the tertiary H in the 9-position of the fluorene moiety, and the substantially down-field shifted signals appearing beyond 8 ppm were mostly assignable to protons around the polycyclic moiety bearing the positive charge.

Finally, the unambiguous structure of **BCHF1+H$^+$**, including the identity of the counter ion, was revealed by X-ray crystallography performed with a single crystal of the red compound (Fig. 3 and S13†). The molecule was shown to have a planar polycyclic skeleton composed of linearly fused 6-5-6-7-6 membered rings, to which two mesityl groups were attached almost perpendicularly *via* the five- and seven-membered rings. Nonetheless, from the bond angles it was perceptible that the 9-position of the fluorene moiety was protonated, assuming the sp^3 hybridization state. Moreover, the counter ion of this protonated structure was identified to be tetrafluoroborate (BF_4^-), which was positioned closer to the centre of the seven-membered ring bearing a positive charge. The average bond length of the seven-membered ring was 1.418 Å, slightly shorter than that found with a dibenzotropylium cation derivative (1.425 Å) reported in the literature.[46] Thus, the calculated harmonic oscillator model of aromaticity (HOMA) index[47] of the seven-membered ring in **BCHF1+H$^+$** (0.52) was also slightly

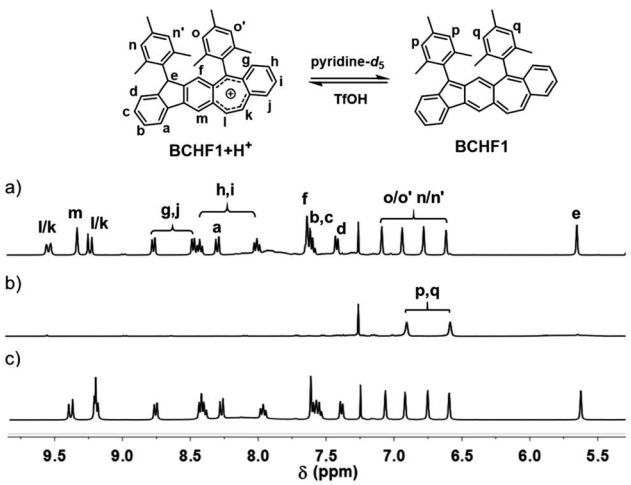

Fig. 2 ^{1}H NMR spectra of **BCHF1+H$^+$** in $CDCl_3$ (a) and upon the addition of pyridine-d_5 (b) followed by excess TfOH acid (c).

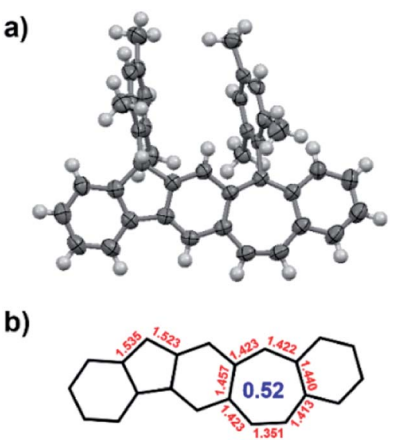

Fig. 3 (a) X-ray crystallographic structure of **BCHF1+H$^+$** (counter ion BF_4^- omitted for clarity); (b) selected bond lengths (Å) and the calculated HOMA index of the seven-membered ring.

higher than that of the dibenzotropylium cation (0.48),[46] suggesting a comparable aromatic character.

Acid/base-responsive properties

Subsequently, acid–base reaction experiments were conducted to examine the properties of neutral **BCHF1**. The reversible deprotonation of **BCHF1+H$^+$** and re-protonation of **BCHF1** were first examined by monitoring the ^{1}H NMR spectral changes in response to consecutive additions of a base and an acid to a solution of **BCHF1+H$^+$**. As the neutral form of **BCHF1** was found to be unstable under ambient conditions, a small amount of deuterated pyridine (pyridine-d_5) was added to the solution of **BCHF1+H$^+$** in $CDCl_3$ under a nitrogen atmosphere. Such sensitivity toward oxygen also corroborated the diradical propensity of **BCHF1**. Upon addition of the base, almost all resonances belonging to **BCHF1+H$^+$** vanished from the ^{1}H NMR spectrum (Fig. 2b), suggesting the formation of a paramagnetic species. Only two aromatic signals remained at about 6.6 and 6.9 ppm, which were assigned to the aromatic protons on two mesityl groups positioned relatively far away from the spins distributed over the polycyclic framework. The fact that four different mesityl protons observed with **BCHF1+H$^+$** merged into two sets in **BCHF1** further corroborated the assumption that deprotonation took place with the sp^3-hybridized carbon-9 of the fluorene unit and resulted in a more symmetrized, planar polycyclic skeleton. Next, an excess amount of trifluoromethanesulfonic acid (TfOH) was added to this solution containing *in situ* generated **BCHF1**, followed by some deuterated water to extract the excess acid and pyridinium triflate salt. After these procedures, all proton resonances characteristic of **BCHF1+H$^+$** were recovered (Fig. 2c), with minor chemical shift variations likely due to the solvent polarity and ionic strength changes. These results clearly verified the occurrence of reversible deprotonation and protonation processes occurring to **BCHF1+H$^+$** and **BCHF1**, and that the latter displayed paramagnetic properties around room temperature, in agreement with the small ΔE_{S-T} predicted by the theoretical calculations.

Next, the absorption spectral features of **BCHF1+H$^+$** and **BCHF1** were examined by varying the pH conditions and compared to those of **BCHF2**. A solution of **BCHF1+H$^+$** in CH_2Cl_2 depicted a series of absorption bands in the UV-visible range from *ca.* 300 to 630 nm (Fig. S1†), which accounted for the red colour of the compound. Upon the addition of pyridine (*ca.* 1000 equiv.), the red colour of the solution turned lighter and the absorption intensity was found to decrease only by about 20%, while the overall spectral band shape remained nearly unchanged (Fig. S2†). Such a phenomenon suggested that the basicity of pyridine was not strong enough to completely deprotonate **BCHF1+H$^+$**. Although in the earlier experiments, most of the ^{1}H NMR signals of **BCHF1+H$^+$** were observed to disappear completely upon treatment with pyridine, it was likely due to the rapid exchange processes between the deprotonated paramagnetic and protonated diamagnetic species. Thus, in order to completely deprotonate **BCHF1+H$^+$**, a stronger base was necessarily applied. We then found that some strongly reductive bases, such as triethylamine (Et_3N), caused noticeable decomposition of **BCHF1**, as evidenced by the partial recovery of the absorption spectra in repeated acid–base titrations (Fig. S2†).

Upon screening a set of different bases, 1,8-diazabicyclo[5.4.0]undec-7-ene (DBU) appeared to offer suitable basicity while entailing minimum decomposition of **BCHF1**. Upon adding *ca.* 2 equiv. DBU to a solution of **BCHF1+H$^+$** in CH_2Cl_2, a drastic colour change from red to green was observed. Meanwhile, the absorption spectrum showed evident changes, with the original band replaced by a completely new set of absorption peaks (Fig. 4). Particularly notable was the emergence of some pronounced long-wavelength absorption activities between 520 and 700 nm, which evidenced the formation of a more delocalized framework featuring a quinoidal/diradical structure, attributable to **BCHF1**. More importantly, the absorption spectrum of **BCHF1+H$^+$** was completely restored when the solution of **BCHF1** was treated with TFA, evidencing the conversion back to **BCHF1+H$^+$**. When a larger amount of DBU was then added to the same solution such as to re-generate **BCHF1**, slightly attenuated absorptivity was observed, indicative of minor decomposition. Overall, **BCHF1** produced by treating **BCHF1+H$^+$** with DBU exhibited decent stability. By continuously monitoring the absorption spectrum, its half-life time in CH_2Cl_2 under a nitrogen atmosphere, in the presence of a minimal amount of DBU, was estimated to be about 35 hours (Fig. S6†).

Analogous to the reversible protonation–deprotonation behaviours demonstrated with **BCHF1**, similar processes were also exhibited by **BCHF2**. The latter displayed completely reversible absorption changes upon reacting with acids and bases (Fig. S4†). Compared to the low-energy band shown by **BCHF1** curtailed at about 700 nm, the long-wavelength absorption of **BCHF2** was extended to over 900 nm (Fig. S1†). Such spectral differences were explained by TD-DFT calculations (Tables S2 and S4†), which indicated that the low-energy transition from the HOMO to the LUMO was allowed for **BCHF2**, but forbidden in **BCHF1**. This might as well be related to the more pronounced diradical nature and considerably smaller ΔE_{S-T} of

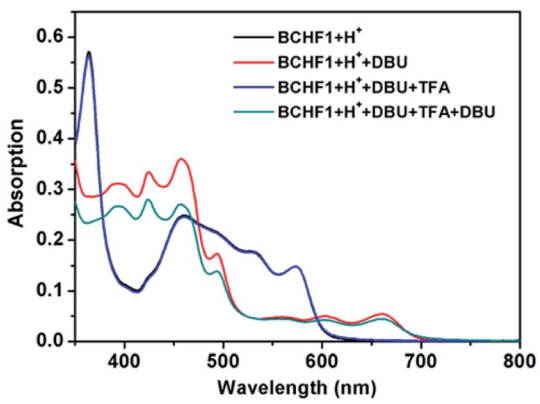

Fig. 4 Absorption spectra of **BCHF1+H$^+$** in CH_2Cl_2 upon sequential additions of DBU, TFA, and DBU again (the black and blue lines overlap almost completely; spectra were collected from the same sample subjected to repeated acid/base additions).

BCHF1. In spite of the similar acid-based responsive spectral behaviours, much differed air stability was observed with **BCHF2**. All the above acid–base reactions were conducted under ambient conditions and no evidence of decomposition was detected even when the solution of **BCHF2** was exposed to a large excess of Et_3N. Such optimal stability was also a good indication that **BCHF2** did not possess observable diradical properties, which was confirmed by its silence in the EPR spectroscopy.

Besides the absorption spectral properties, both molecules also manifested distinctive fluorescence emission responses to pH changes. The protonated form of **BCHF1+H$^+$** was found to be highly emissive in solution by showing an intense fluorescence band around 600 nm. The fluorescence was found to be completely quenched upon de-protonation with DBU (Fig. S5†). The non-emissive properties were consistent with the diradical characteristic of **BCHF1**. Upon adding TFA to the solution, the emission band was restored. Similarly, the neutral form of **BCHF2** was non-emissive in solution, but an intense emission band was observed around 640 nm upon treatment with TFA, which could be quenched again with excessive Et_3N (Fig. S4†).

Next, the pH-sensitive magnetic-switching behaviours were investigated with EPR spectroscopy. While **BCHF2** was completely EPR silent, the conjugated acid–base pair of **BCHF1+H$^+$**/**BCHF1** demonstrated clearly pH-responsive EPR intensity changes (Fig. 5). As a diamagnetic molecule, **BCHF1+H$^+$** unsurprisingly showed no EPR signal in CH_2Cl_2 solution. When 2 equiv. DBU was added to this solution, a conspicuous paramagnetic resonance signal immediately appeared at $g = 2.0032$, which was assignable to *in situ* generated **BCHF1**. Then, upon the addition of 20 equiv. TFA to the same solution the EPR signal vanished, again. Subsequently, by adding 20 more equivalents of DBU the EPR signal clearly regenerated, with its intensity very close to that of the first time (Fig. S7†). This entire process was in complete consistency with the absorption spectral changes observed earlier (Fig. 4). The slight EPR intensity drop, indicative of minor **BCHF1** decomposition, was mainly due to the relatively large amount of DBU necessarily applied to neutralize excess TFA. Hence, we turned to a different acid, *p*-toluenesulfonic acid (TsOH) with a pK_a value better matching the pK_b of DBU, such that minimized amounts of acids and bases could be used to achieve better reproducibility in the repeated interconversion between **BCHF1** and **BCHF1+H$^+$**, for inducing minimal decomposition. Next, by successively adding a finite amount of DBU (2 equiv.) followed by TsOH (2 equiv.), many more cycles of switching between the "on" and "off" states of the EPR signal were realized (Fig. 5 and S3†). These experiments very well demonstrated that **BCHF1** could be swapped reversibly between the deprotonated paramagnetic and protonated diamagnetic forms *via* the dynamic acid/base reactions in response to pH changes.

Next, the intrinsic magnetic properties of **BCHF1** were investigated. A featureless EPR signal with a *g* factor of 2.0036 was produced by **BCHF1** in the solid state (Fig. 6a). The intensity

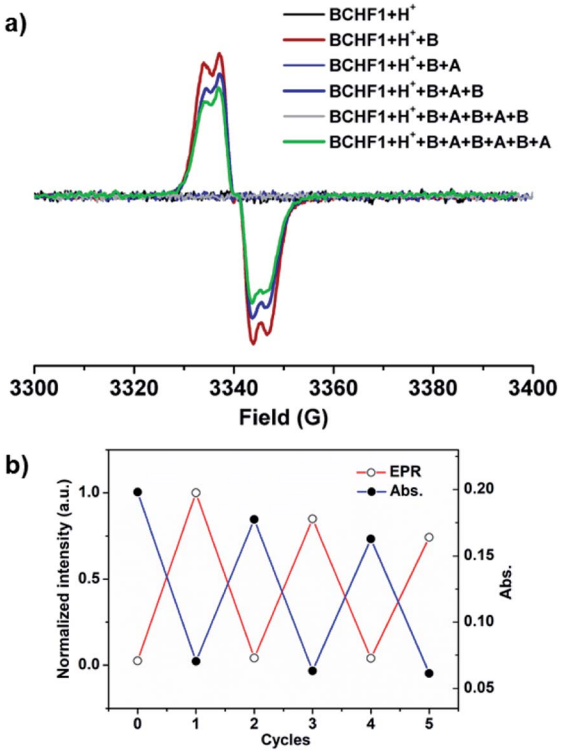

Fig. 5 (a) EPR spectra of **BCHF1+H$^+$** in CH_2Cl_2 upon three cycles of the addition of 2 equiv. DBU (B) followed by 2 equiv. TsOH (A); (b) normalized EPR (@3336 G) and absorption (@570 nm) intensity changes in each cycle.

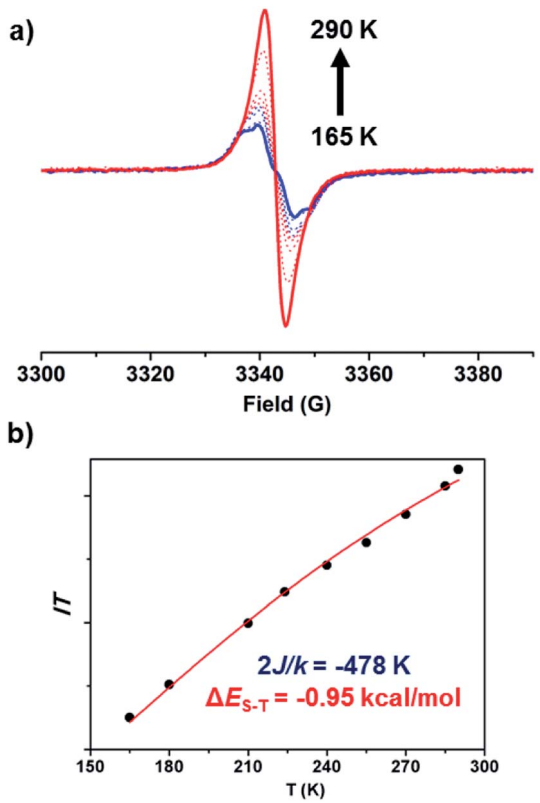

Fig. 6 (a) Varied-temperature EPR spectra of **BCHF1** in the solid state (obtained by treating **BCHF1+H$^+$** in CH_2Cl_2 with 2 equiv. DBU followed by evaporation under an inert atmosphere); (b) plot of *IT vs. T* (*I*, double integral of the EPR signal; the fitting curve shown as a red line).

of this resonance peak was observed to decrease at lowered temperatures, indicating the existence of a singlet ground state with a thermally accessed triplet state. By fitting the values of *IT* as a function of *T* using the modified Bleaney–Bowers equation (Fig. 6b),[48] a ΔE_{S-T} value of −0.95 kcal mol^{-1} was estimated for **BCHF1**, which was in a reasonable agreement with the calculated value (−1.84 kcal mol^{-1}). Also, such a singlet–triplet energy gap was much smaller compared to those reported for various studied indeno-fluorene isomers,[28,43] suggesting that a more pronounced diradical propensity was manifested by **BCHF1**.

In light of its impressive pH-sensitive magnetic switching properties illustrated in solution, the capability of **BCHF1+H$^+$** for responding to gaseous acids and bases in the solid state was also tested. First, a thin film of **BCHF1+H$^+$** was prepared by evaporating its CH_2Cl_2 solution under a nitrogen atmosphere. Then, the vapour of DBU was introduced to induce a reaction with the film. The dark red film was observed to turn green gradually over 5 minutes. The absorption spectrum change, particularly the emergence of the peak around 670 nm, clearly indicated the formation of **BCHF1** in the thin film (Fig. S9†). Subsequently, the film was exposed to the vapour of TFA, and its green colour quickly turned back to dark red in merely one minute, with the absorption spectrum restored to the protonated state as well. The faster kinetics observed with re-protonation was assumed to be related to the higher vapour pressure of TFA. These deprotonation and re-protonation processes were also monitored with EPR spectroscopy. A clear rise in the EPR signal was detected when the thin film of **BCHF1+H$^+$** was exposed to DBU vapour, and a complete silence of the resonance signal was also recorded when the film was then exposed to the TFA vapour (Fig. S9b†).

Conclusions

In summary, by integrating a quinoid moiety with azulene, a novel non-alternant hydrocarbon **BCHF1** featuring multi-facet zwitterionic and diradical properties was designed. By virtue of the zwitterionic feature conferred by the azulene-like structure, **BCHF1** easily adopted a proton and formed a stable compound in its conjugated acid salt state (*i.e.*, **BCHF1+H$^+$**). This salt was successfully isolated and characterized by ^{1}H NMR spectroscopy and single-crystal X-ray crystallography. It could be converted to its neutral form of **BCHF1** by reacting with organic bases, such as DBU. The diradical properties of **BCHF1**, featuring a small ΔE_{S-T}, were clearly evidenced by the conspicuous EPR signal detectable around room temperature, since the closed-shell quinoidal and zwitterionic states should both be EPR silent. The varied-temperature EPR experiments further revealed an impressively small ΔE_{S-T} of *ca.* −0.95 kcal mol^{-1} for **BCHF1**, indicative of a singlet ground state with a thermally accessed triplet state. By monitoring the recurrent disappearance and re-appearance of ^{1}H NMR and EPR signals in response to repeated additions of acids and bases to the solutions of **BCHF1+H$^+$**, the molecule was clearly demonstrated to undergo reversible deprotonation and protonation reactions, thereby switching between the paramagnetic and diamagnetic forms. Additionally, the thin film of **BCHF1+H$^+$/BCHF1** was shown to be responsive to the vapour of DBU and TFA by manifesting dramatic absorption changes and reversibly turning on and off its EPR signal. Basically, by harnessing a dynamic protonation process of a unique zwitterionic/diradical molecule, a pH-controlled switching mechanism between the paramagnetic and diamagnetic states was realized. To the best of our knowledge, this is the first example of a PAH showing acid/base-responsive magnetic-switching properties, which is envisioned to open up new opportunities for designing stimuli-responsive organic magnetic materials.

Conflicts of interest

There are no conflicts to declare.

Acknowledgements

The work is financially supported by the National Natural Science Foundation of China (Nos 21925501, 21790363 and 21674001) and the Beijing National Laboratory for Molecular Sciences (BNLMS-CXXM-201902). The support from the High-performance Computing Platform of Peking University for the computational resources and the Steady High Magnetic Field Facilities, High Magnetic Field Laboratory, CAS is acknowledged.

Notes and references

1 A. Rajca, *Chem. Rev.*, 1994, **94**, 871–893.
2 A. Rajca, J. Wongsriratanakul and S. Rajca, *Science*, 2001, **294**, 1503–1505.
3 M. E. Itkis, X. Chi, A. W. Cordes and R. C. Haddon, *Science*, 2002, **296**, 1443–1445.
4 X. Yu, A. Mailman, K. Lekin, A. Assoud, C. M. Robertson, B. C. Noll, C. F. Campana, J. A. K. Howard, P. A. Dube and R. T. Oakley, *J. Am. Chem. Soc.*, 2012, **134**, 2264–2275.
5 A. Coskun, A. J. M. Spruell, G. Barin, W. R. Dichtel, A. H. Flood, Y. Y. Botros and J. F. Stoddart, *Chem. Soc. Rev.*, 2012, **41**, 4827–4859.
6 Q. Peng, A. Obolda, M. Zhang and F. Li, *Angew. Chem., Int. Ed.*, 2015, **54**, 7091–7095.
7 I. Ratera and J. Veciana, *Chem. Soc. Rev.*, 2012, **41**, 303–349.
8 N. Tanifuji, M. Irie and K. Matsuda, *J. Am. Chem. Soc.*, 2005, **127**, 13344–13353.
9 J. Wang, L. Hou, W. R. Browne and B. L. Feringa, *J. Am. Chem. Soc.*, 2011, **133**, 8162–8164.
10 K. Lekin, H. Phan, S. M. Winter, J. W. L. Wong, A. A. Leitch, D. Laniel, W. Yong, R. A. Secco, J. S. Tse, S. Desgreniers, P. A. Dube, M. Shatruk and R. T. Oakley, *J. Am. Chem. Soc.*, 2014, **136**, 8050–8062.
11 W. Fujita and K. Awaga, *Science*, 1999, **286**, 261–262.
12 D. A. Shultz, R. M. Fico, P. D. Boyle and J. W. Kampf, *J. Am. Chem. Soc.*, 2001, **123**, 10403–10404.
13 J. L. Brusso, O. P. Clements, R. C. Haddon, M. E. Itkis, A. A. Leitch, R. T. Oakley, R. W. Reed and J. F. Richardson, *J. Am. Chem. Soc.*, 2004, **126**, 8256–8265.

14 M. B. Mills, T. Wohlhauser, B. Stein, W. R. Verduyn, E. Song, P. Dechambenoit, M. Rouzieres, R. Clerac and K. E. Preuss, *J. Am. Chem. Soc.*, 2018, **140**, 16904–16908.
15 G. Gryn'ova, D. L. Marshall, S. J. Blanksby and M. L. Coote, *Nat. Chem.*, 2013, **5**, 474–481.
16 T. Krchova, V. Herynek, A. Galisova, J. Blahut, P. Hermann and J. Kotek, *Inorg. Chem.*, 2017, **56**, 2078–2091.
17 Y. Li, X. Lei, S. Jockusch, J. Y.-C. Chen, M. Frunzi, J. A. Johnson, R. G. Lawler, Y. Murata, M. Murata, K. Komatsu and N. J. Turro, *J. Am. Chem. Soc.*, 2010, **132**, 4042–4043.
18 D. Bardelang, G. Casano, F. Poulhes, H. Karoui, J. Filippini, A. Rockenbauer, R. Rosas, V. Monnier, D. Siri, A. Gaudel-Siri, O. Ouari and P. Tordo, *J. Am. Chem. Soc.*, 2014, **136**, 17570–17577.
19 A. C. Fahrenbach, Z. Zhu, D. Cao, W. Liu, H. Li, S. K. Dey, S. Basu, A. Trabolsi, Y. Y. Botros, W. A. Goddard and J. F. Stoddart, *J. Am. Chem. Soc.*, 2012, **134**, 16275–16288.
20 S. Venkataramani, U. Jana, M. Dommaschk, F. D. Sönnichsen, F. Tuczek and R. Herges, *Science*, 2011, **331**, 445–448.
21 F. Touti, P. Maurin and J. Hasserodt, *Angew. Chem., Int. Ed.*, 2013, **52**, 4654–4658.
22 B. P. Timko, T. Dvir and D. S. Kohane, *Adv. Mater.*, 2010, **22**, 4925–4943.
23 H. Lee, T. Shin, J. Cheon and R. Weissleder, *Chem. Rev.*, 2015, **115**, 10690–10724.
24 M. Nakano and B. Champagne, *J. Phys. Chem. Lett.*, 2015, **6**, 3236–3256.
25 Y. Morita, S. Suzuki, K. Sato and T. Takui, *Nat. Chem.*, 2011, **3**, 197–204.
26 Z. Sun, Q. Ye, C. Chi and J. Wu, *Chem. Soc. Rev.*, 2012, **41**, 7857–7889.
27 Z. Zeng, X. Shi, C. Chi, J. T. L. Navarrete, J. Casado and J. Wu, *Chem. Soc. Rev.*, 2015, **44**, 6578–6596.
28 G. E. Rudebusch, J. L. Zafra, K. Jorner, K. Fukuda, J. L. Marshall, I. Arrechea-Marcos, G. L. Espejo, R. P. Ortiz, C. J. Gómez-García, L. N. Zakharov, M. Nakano, H. Ottosson, J. Casado and M. M. Haley, *Nat. Chem.*, 2016, **8**, 753–759.
29 A. Konishi, Y. Okada, M. Nakano, K. Sugisaki, K. Sato, T. Takui and M. Yasuda, *J. Am. Chem. Soc.*, 2017, **139**, 15284–15287.
30 M. R. Ajayakumar, Y. Fu, J. Ma, F. Hennersdorf, H. Komber, J. J. Weigand, A. Alfonsov, A. A. Popov, R. Berger, J. Liu, K. Müllen and X. Feng, *J. Am. Chem. Soc.*, 2018, **140**, 6240–6244.
31 Z. Zhang, G. M. Ferrence and T. D. Lash, *Org. Lett.*, 2009, **11**, 101–104.
32 Y. Yamaguchi, M. Takubo, K. Ogawa, K. Nakayama, T. Koganezawa and H. Katagiri, *J. Am. Chem. Soc.*, 2016, **138**, 11335–11343.
33 E. Puodziukynaite, H. W. Wang, J. Lawrence, A. J. Wise, T. P. Russell, M. D. Barnes and T. Emrick, *J. Am. Chem. Soc.*, 2014, **136**, 11043–11049.
34 Y. Sasaki, M. Takase, T. Okujima, S. Mori and H. Uno, *Org. Lett.*, 2019, **21**, 1900–1903.
35 M. Murai, S. Iba, H. Ota and K. Takai, *Org. Lett.*, 2017, **19**, 5585–5588.
36 H. Xin and X. Gao, *ChemPlusChem*, 2017, **82**, 945–956.
37 K. H. Grellmann, E. Heilbronner, P. Seiler and A. Weller, *J. Am. Chem. Soc.*, 1968, **90**, 4238–4242.
38 X. B. Wang, J. K.-P. Ng, P. Jia, T. Lin, C. M. Cho, J. Xu, X. Lu and C. He, *Macromolecules*, 2009, **42**, 5534–5544.
39 E. Amir, R. J. Amir, L. M. Campos and C. J. Hawker, *J. Am. Chem. Soc.*, 2011, **133**, 10046–10049.
40 X. Yang, X. Shi, N. Aratani, T. P. Goncalves, K.-W. Huang, H. Yamada, C. Chi and Q. Miao, *Chem. Sci.*, 2016, **7**, 6176–6181.
41 M. Abe, *Chem. Rev.*, 2013, **113**, 7011–7088.
42 A. Shimizu and Y. Tobe, *Angew. Chem., Int. Ed.*, 2011, **50**, 6906–6910.
43 A. Shimizu, R. Kishi, M. Nakano, D. Shiomi, K. Sato, T. Takui, I. Hisaki, M. Miyata and Y. Tobe, *Angew. Chem., Int. Ed.*, 2013, **52**, 6076–6079.
44 J. J. Dressler, Z. Zhou, J. L. Marshall, R. Kishi, S. Takamuku, Z. Wei, S. N. Spisak, M. Nakano, M. A. Petrukhina and M. M. Haley, *Angew. Chem., Int. Ed.*, 2017, **56**, 15363–15367.
45 D. T. Chase, A. G. Fix, B. D. Rose, C. D. Weber, S. Nobusue, C. E. Stockwell, L. N. Zakharov, M. C. Lonergan and M. M. Haley, *Angew. Chem., Int. Ed.*, 2011, **50**, 11103–11106.
46 A. Konishi, K. Horii, D. Shiomi, K. Sato, T. Takui and M. Yasuda, *J. Am. Chem. Soc.*, 2019, **141**, 10165–10170.
47 T. M. Krygowski and M. K. Cyranski, *Chem. Rev.*, 2001, **101**, 1385–1419.
48 Y. Matsuta, D. Sakamaki, R. Kurata, A. Ito and S. Seki, *Chem.–Asian J.*, 2017, **12**, 1889–1894.